Effect of organometallic clamp properties on the apparent diversity of tensile response of nanowires

2013 Nanotechnology 24 235704

(http://iopscience.iop.org/0957-4484/24/23/235704)

Nanotechnology **24** (2013) 235704 (8pp) doi:10.1088/0957-4484/24/23/235704

Effect of organometallic clamp properties on the apparent diversity of tensile response of nanowires

Kathryn F Murphy, Lisa Y Chen and Daniel S Gianola

Department of Materials Science and Engineering, University of Pennsylvania, 3231 Walnut Street, Philadelphia, PA 19104, USA

E-mail: gianola@seas.upenn.edu

Received 21 February 2013, in final form 5 April 2013
Published 13 May 2013
Online at stacks.iop.org/Nano/24/235704

Abstract
The influence of the experimental boundary conditions used for tensile testing of individual nanowires on the measured apparent mechanical response is reported. Using a microelectromechanical platform designed for *in situ* tensile testing, in combination with digital image correlation of sequences of scanning electron microscope images, the mechanical behavior of single crystalline Si, Pd, and $Ge_2Sb_2Te_5$ nanowires was measured during load–unload cycles. *In situ* testing enables direct determination of the nanowire strain. Comparison of the direct strain with common metrics for apparent strain that include any compliance or slipping of the clamping materials (electron-beam induced Pt-containing deposits) highlights several different artifacts that may be manifested. Calculation of the contact stiffness is thus enabled, providing guidelines for both proper strain measurement and selection of clamping materials and geometries that facilitate elucidation of intrinsic material response. Our results suggest that the limited ability to tailor the stiffness of electron-beam induced deposits results from the predominance of the organic matrix in controlling its mechanical properties owing to relatively low Pt content and sparse morphology.

(Some figures may appear in colour only in the online journal)

1. Introduction

The need to accurately determine the mechanical behavior of nanowires and nanotubes is predicated on developing predictable and reliable devices employing quasi-one-dimensional nanostructures (hereafter referred to as nanowires) as functional building blocks. Many such nanoscale elements are subjected to extreme mechanical duress during routine use in applications such as nanoelectromechanical (NEMS) devices, electrodes for energy storage devices [1–3], and novel atomic force microscope (AFM) tips [4–6]. Many experimental techniques have consequently been developed in recent years to accurately interrogate the mechanical response of nanowires, which often show behavior distinct from that of their bulk material counterparts. The most direct methods of mechanical testing use nominally uniaxial states of stress, which yield the most accurate measurements of mechanical properties owing to a uniform stress state with relatively weak dependence on geometry, which is often difficult to properly measure and thus can contribute strongly to measurement uncertainties associated with difficult nanoscale measurements. Moreover, tensile testing modalities circumvent problems associated with compressive testing such as contact friction and stress gradients near the specimen gage section. Accordingly, a number of experimental schemes for applying displacement and measuring load on individual nanowires in tensile geometries have been devised. Among these are microelectromechanical systems (MEMS)-based devices [7–14], push-to-pull devices [15–17], and systems consisting of a nanomanipulator and a cantilever load cell [18–21] or two AFM cantilevers [22]. Specimen strain has been determined in a variety of ways, e.g. measuring the displacement between the edges of the grips from electron micrographs [7–9, 17, 22], using digital image

correlation (DIC) of optical [14] or scanning electron microscope (SEM) [13, 14, 16, 19, 21] images, using capacitative sensors [10–12], or using a nanoindenter [15]. Despite significant advances in such techniques, the large range of properties and behavior reported from nanowire measurements suggests the role of testing artifacts beyond the errors due to measurement of nanowire geometry alone.

Central to the establishment of a tensile stress within a specimen are strong and stiff clamps that properly secure the nanowire to the testing grips. A large fraction [7–10, 12–14, 16–22] of the aforementioned nanowire tensile testing methods rely on mechanical clamps synthesized by electron-beam induced deposition (EBID) of either contaminant hydrocarbons present in the SEM chamber via surface decomposition, or EBID or ion-beam induced deposition (IBID) from an organometallic precursor gas containing platinum, gold, tungsten, copper, molybdenum, iron, or cobalt [23]. The properties, in particular the stiffnesses, of these clamps are critically important since strain is often measured using the grip displacement [7, 8, 10–13, 15, 17–22]; any deformation of the clamps would be incorporated into the apparent deformation of the specimen. Some experimental work has been performed measuring the stiffness of the clamping material itself. For instance, the Young's modulus of metal-free EBID deposits was found to be in the range of 34–60 GPa [24], and the Young's modulus of Cu-containing deposits in the range of 16–27 GPa [25]. In these reports, measurements of Young's moduli of the EBID materials were considerably lower than those of the inorganic materials commonly tested. Further evidence that the finite stiffness of nanoscale clamps will affect measured mechanical response is the demonstrated effect of EBID clamp size on the Young's modulus measured using resonance techniques [26]. Despite the widespread use in the vast majority of reports on nanowire and nanotube modulus, to our knowledge no work has directly demonstrated the range of distinct apparent nanowire behavior resulting from improper consideration of tensile boundary conditions, quantitatively measured the contact stiffness of these clamps as deposited on tensile testing specimens, or provided guidelines for a proper clamp stiffness necessary for accurate measure of Young's modulus in nanowires.

In this paper, we employ MEMS-based tensile testing and DIC to *directly* measure strain in Si, Pd, and $Ge_2Sb_2Te_5$ nanowires clamped with electron-beam deposited Pt- and W-containing clamps. By comparing the direct and nominal measurements of strain to calculate real and effective Young's moduli, respectively, we determine the stiffness of the clamps and their influence on the measured mechanical response of the nanowires. We furthermore show that accuracy of measured nanowire properties is dependent on nanowire geometry and clamping configuration but not measurably on electron-beam parameters used for deposition or metal content of the clamp.

2. Experimental methods

The MEMS device shown in figure 1 was used to perform uniaxial tensile tests on individual inorganic nanowires.

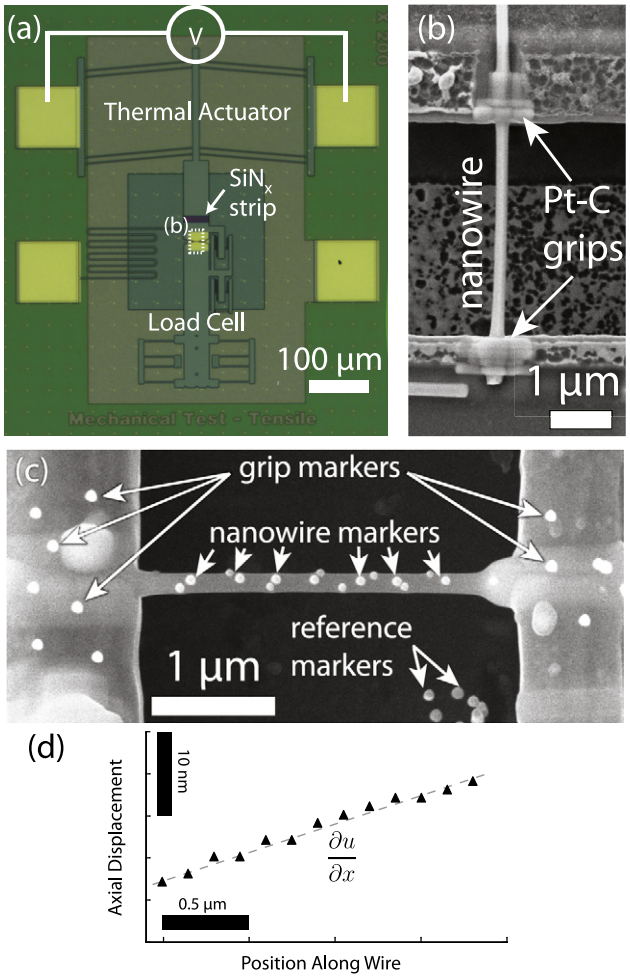

Figure 1. (a) MEMS tensile platform employed for *in situ* testing of individual nanowires. (b) SEM image showing $Ge_2Sb_2Te_5$ nanowire suspended across testing grips and secured using EBID clamps. (c) Scheme for direct measurement of nanowire strain during testing using digital image correlation of markers providing (d) axial displacements along the gage section of the nanowire.

Displacement was applied by a suspended thermal actuator and load was determined by measuring the displacement of a compound flexure beam system with a stiffness of 44 N m^{-1}. Trenches were milled into the grips of the device using a focused ion beam (FIB) to facilitate proper alignment of the specimen with the device. Individual single-crystal nanowires of Si (vapor–liquid–solid-grown, ⟨111⟩-oriented purchased from Sigma Aldrich, as well as top-down fabricated, ⟨100⟩-oriented patterned using electron-beam lithography and etched following the methods of [27, 28]), Pd (⟨110⟩-oriented [19]), and $Ge_2Sb_2Te_5$ (⟨$10\bar{1}0$⟩-oriented [29, 30]) were harvested inside an SEM from their as-grown or as-deposited state by attaching a nanomanipulator to a single nanowire using a small amount of Pt-containing EBID material (precursor of methylcyclopentadienyl platinum trimethyl). The isolated nanowires were then aligned to the grips of the MEMS device, lowered into the trenches (except specimens Si B and F and Pd D, E, and H, which were placed flat on the grips), and clamped using EBID (figure 1(b)). Pt- or W-containing (precursor of $W(CO)_6$) clamps were deposited

Table 1. Geometry of nanowires and EBID clamps used for tensile testing, in addition to measured values of wire and contact stiffnesses and Young's moduli. Values of Young's moduli are tabulated as calculated based on direct measurement of strain in the wire gage section and indirect values based on the relative grip displacement.

Wire	d (nm)	L (μm)	Clamp geometry	Contact length (μm)	Deposition voltage (kV)	Beam current (pA)	k_{wire} (kN m^{-1})	$k_{contact}$ (kN m^{-1})	$\frac{k_{contact}}{k_{wire}}$	E_{direct} (GPa)	$E_{apparent}$ (GPa)	Modulus error (%)
Si⟨100⟩A	165	3.2	Trench	0.80	5	40	0.86	6.8	8.1	129	103	20
Si⟨100⟩B	165	1.1	Flat	0.60	10	40	2.4	12	4.9	123	87	29
Si⟨111⟩C	180	7.1	Trench	0.65	5	40	0.67	2.3	3.4	188	118	37
Si⟨111⟩D	171	7.1	Trench	1.8	5	40	0.63	3.2	5.0	194	139	28
Si⟨111⟩E	172	7.1	Trench[a]	1.0	5	560	0.63	2.0	3.3	192	118	39
Si⟨111⟩F	176	7.0	Flat	1.1	5	40	0.76	3.7	4.9	219	156	29
Pd A	77	7.1	Trench	0.45	10	40	0.08	1.6	21	114	104	9
Pd B	63	3.0	Trench	0.45	10	40	0.14	1.5	10	139	116	17
Pd C	100	3.2	Trench	0.28	20	40	0.31	1.6	5.3	127	92	27
Pd D	33	3.0	Flat	0.50	10	40	0.07	1.1	15	243	215	12
Pd E	62	3.1	Flat	0.32	20	40	0.13	34	262	132	131	0.7
Pd F	37	1.47	Trench	0.58	2	420	0.09	0.57	6.0	130	97	25
Pd G	88	3.34	Trench	0.31	20	40	0.21	2.0	9.5	115	95	17
Pd H	100	3.34	Flat	0.33	5	40	0.29	6.1	21	125	114	9
$Ge_2Sb_2Te_5$ A	280	3.4	Trench	0.80	10	40	0.71	7.9	11	39	33	16
$Ge_2Sb_2Te_5$ B	130	6.7	Trench	1.0	5	40	0.09	1.3	14	47	41	12
$Ge_2Sb_2Te_5$ C	115	2.8	Trench	0.38	10	40	0.20	2.6	13	53	46	13

[a] Tungsten-containing deposition used for clamping. All other clamps were platinum-containing.

at 2–20 kV accelerating voltages and 40 or 420 pA (for Pt deposition) or 560 pA (for W deposition) beam currents at room temperature. These precursor materials and deposition conditions are known to produce carbon-rich deposits with Pt content varying from 5 to 16 at.% [31]. In the case of W, the reported metal content for 5 kV accelerating voltage and 1.6 nA beam current—3 times the beam current used here—is about 35 at.% [32]. The deposition time was chosen to produce clamps with thicknesses that exceeded the nanowire diameter. Clamp widths ranged from 0.5 to 1.5 μm and lengths along the wire ranged from 0.3 to 1.8 μm. Once secured, the nanomanipulator was retracted, breaking the relatively weaker bond between the manipulator and the wire without applying stress to the specimen gage section. Details of the wire materials, dimensions, EBID conditions, and clamping configurations are summarized in table 1.

In order to measure load and displacement using digital image correlation, contrast-producing markers were deposited using EBID in spot mode on both grips, the substrate, and along the length of the wire spaced far enough apart to prevent load bearing (figure 1(c)). Strain rates between 10^{-5} and 10^{-4} s^{-1} were applied and series of SEM images were obtained continuously during *in situ* testing. Displacements of the markers placed on the wire, the actuator, the load cell, and on the substrate beneath the suspended grips were determined from DIC of the SEM image series with resolution better than 0.1 pixels or 1 nm. Engineering strain in the nanowire was measured from displacement gradients (figure 1(d)) obtained from markers placed directly on the nanowire, while the effective engineering strain was measured from the relative displacements of the two grips and the original gauge length. Measurements of the apparent modulus before and after depositing markers directly on the wire showed no change, indicating that any stiffening due to spot deposition was negligible. Displacements of the load cell, and hence the forces, were determined from the relative displacements of the load cell-side grip and the substrate (from intentionally placed reference markers). Stress–strain curves demonstrating the repeatability of the measured response using the direct measurement of strain on a single ⟨110⟩ Pd wire are shown in figure 2(a) via two consecutive load–unload cycles and subsequent loading to fracture. Young's moduli were measured from the unloading portions of the stress–strain curves to avoid incorporation of microplasticity in the measured values. In the case of Pd, which shows pronounced nonlinear elasticity [14], the Young's moduli were measured in the small strain limit.

3. Results and discussion

The diversity of the apparent tensile response in several inorganic nanowires is highlighted in figure 2(b) via representative stress–strain curves. Several distinct manifestations of the role of clamp deformation were measured. The Pd nanowire shown exhibits an apparent difference in modulus using the two strain measurement approaches, although linear elastic behavior is measured with both strain measurement methods, suggesting a low clamp stiffness relative to the nanowire. In contrast, both slight and extreme apparent hysteresis is detected in the Si and $Ge_2Sb_2Te_5$ stress–strain curves, respectively, that vanishes or diminishes in the stress–strain curves obtained from direct strain measurements. This discrepancy can be attributed to permanent deformation of the clamping material or sliding of the nanowire within the clamp. Without a direct measurement of strain, such stress–strain curves could be improperly interpreted as indicating plastic deformation in the nanowires, when in fact the true material deformation remained entirely (Si) or mostly ($Ge_2Sb_2Te_5$)

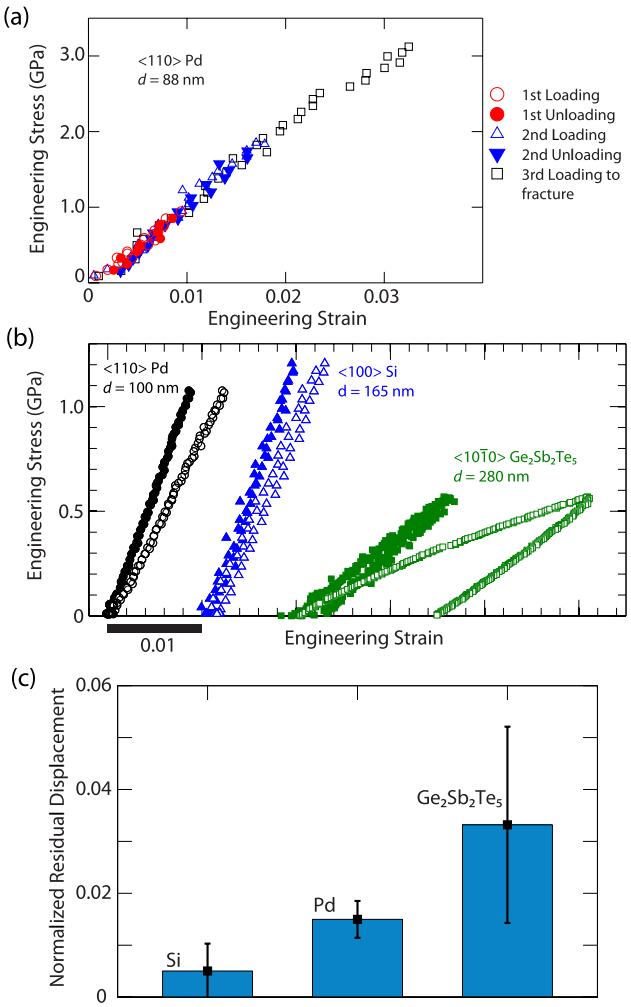

Figure 2. (a) Tensile engineering stress–strain curves for a single ⟨110⟩ Pd nanowire ($d = 88$ nm) for two consecutive load–unload cycles and subsequent loading to fracture, demonstrating the repeatability of the elastic response when using the direct strain measurement approach. (b) Stress–strain curves for nanowires composed of three different inorganic materials highlighting differences between apparent (open markers) and true (closed markers) response upon directly measuring strain within the specimen gage section. Curves for different materials are shifted along the strain axis for clarity. Young's moduli were measured from the unloading portion of the stress–strain curves. (c) In cases where apparent hysteresis was detected, the residual displacement upon unloading normalized by the total applied displacement for the three different tested materials. The apparent material dependence on the residual displacement is consistent with an interfacial sliding mechanism.

elastic. It is important to note that the stress–strain curves shown in figure 2(b) do not indicate the behavior observed in *all* nanowires of a particular material system. Specifically, slight hysteresis was observed in some measurements of Pd nanowires, and not all $Ge_2Sb_2Te_5$ nanowires exhibited large hysteresis.

The occurrence of apparent hysteresis in the stress–strain response of many of the tested nanowires, as quantified by measurements of the residual strain upon unloading, can be ascribed to two potential mechanisms. The first is plastic deformation of the clamping material, which would

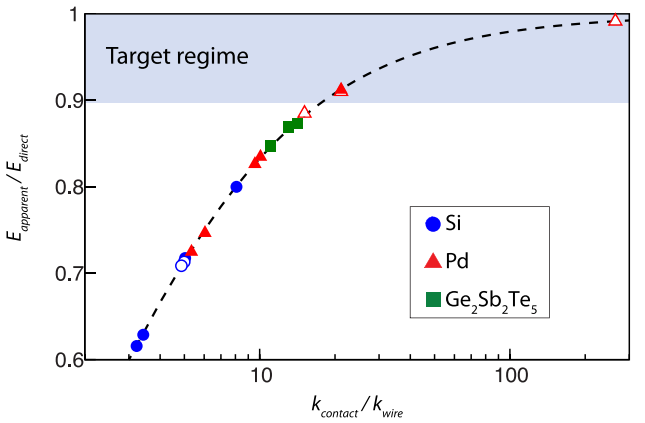

Figure 3. Ratio of apparent to direct measurements of Young's moduli during tensile testing of three different inorganic nanowires versus ratio of contact to wire stiffness. Open symbols denote flat-geometry contacts. The shaded region denotes the optimal range where measurements using remote displacement sensing modes give a value of E_{apparent} that are within 10% of E_{direct} according to equation (1).

be expected to scale with the load transferred by the nanowire to the clamping material. However, measurements of the residual grip displacement (contributing to hysteretic behavior) normalized by the total applied displacement show an inverse correlation. For instance, contacts used for Si and $Ge_2Sb_2Te_5$ nanowires had similar interfacial areas, yet Si nanowires showed the lowest hysteresis despite incurring the largest forces during testing. A second proposed mechanism is interfacial sliding (i.e. pull out) of the nanowire relative to the grips, which presumably depends on the nature of the interfacial bonding. Indeed, the normalized residual displacements showed differences between the three materials (figure 2(c)), with $Ge_2Sb_2Te_5$ and Si showing the highest and lowest values, respectively. However, further experiments would be needed to validate this hypothesis with greater statistical significance.

In addition to measurements of plastic deformation in the clamps, we can determine elastic deformation via measurements of the effective and actual Young's moduli. The mean single contact stiffness may be calculated as

$$k_{\text{contact}} = 2\left(\frac{1}{k_{\text{apparent}}} - \frac{1}{k_{\text{wire}}}\right)^{-1} \qquad (1)$$

where $k_{\text{apparent}} = AE_{\text{apparent}}/L$ and $k_{\text{wire}} = AE_{\text{direct}}/L$, with A and L the cross-sectional area and length of the nanowire, respectively, and E_{apparent} and E_{direct} the moduli determined using the strain from grip displacement and the directly measured strain, respectively. This model provides insight on the influence of the contact stiffness on the apparent elastic response. Namely, the ratio of contact to nanowire stiffnesses must be greater than 18 to yield better than 90% accuracy in measurement of Young's modulus (approximately within our experimental uncertainty considering force and area measurement, see [14]), as shown in figure 3. The resulting stiffnesses, moduli, and errors for Si, Pd, and $Ge_2Sb_2Te_5$ nanowires using the two methods of measuring strain are

summarized in table 1. By varying the nanowire material and geometry we achieved nanowire stiffnesses that varied by over an order of magnitude (0.07–2.4 kN m^{-1}). In total, we found that clamp compliance led to errors in modulus greater than 10% for 14 out of the 17 samples tested, while errors less than 10% were only observed for nanowires with stiffness below approximately 0.3 kN m^{-1}. Contact stiffness was found to be invariant with load for each test, and displayed no correlative trends with contact length along the wire, accelerating voltage during deposition, or nanowire material. Surprisingly, no strong correlation was measured between contact stiffness and beam power, which is known to control the overall metal content in such deposits.

Direct strain measurements yielded Young's moduli for Si⟨111⟩ and ⟨100⟩ that are in excellent agreement with the bulk values (188 and 130 GPa, respectively). Size effects on the elastic behavior would be expected to be negligible for Si nanowires with the diameters tested. Indeed, Zhu *et al* found that nanowire modulus was constant for diameters above 40 nm [18], consistent with our finding of size-independent elastic behavior for our range of sizes. The notable outlier is Si F, a ⟨111⟩ nanowire with a measured E_{direct} of 219 GPa, which was due to poor out-of-plane alignment observed in tilted SEM imaging, resulting in an artificially low strain measurement. Nevertheless, E_{apparent} for this specimen was still 20–39% lower than E_{direct} due to deformation of the clamp, reinforcing the compounding effects of contact compliance. All other tested wires did not show evident signs of such misalignment. We next consider the behavior of $Ge_2Sb_2Te_5$ nanowires. As this study represents the first report on the mechanical behavior of such nanowires, we compare our results with measurements of the biaxial modulus of $Ge_2Sb_2Te_5$ thin films giving Young's modulus of 26 [33] to 32 [34] GPa (assuming a Poisson's ratio of 0.3), slightly lower than our nanowire measurements. The error in modulus measurements for these wires are much lower than for Si due to the decreased nanowire modulus and hence stiffness. With Pd nanowires, the small-strain directly measured moduli for these wires agree well with the bulk Young's modulus of ⟨110⟩ Pd (136 GPa) for nanowire diameters greater than 70 nm, where size-dependent elastic behavior is not expected to arise. Below 70 nm, direct strain measurements show increasing Young's modulus in the Pd nanowires that is a material effect, as discussed in detail in [14]. The Pd nanowires exhibited the largest range in contact stiffness and hence in Young's modulus error.

For all wires in which the clamping geometry was flat, the contact stiffness was approximately equal to (in the case of Si) or greater than or equal to (up to an order of magnitude in the case of Pd) that of the trenched geometry contacts. We ascribe this to the lack of contact in the trenched geometry between the nanowire and the grips such that they were surrounded on all sides by EBID material (see figure 4). For Pd nanowires, using a flat clamping geometry sufficiently increased the clamp stiffness such that E_{apparent} was within 1% of E_{direct}. However, for the Si nanowires, which were much stiffer, the error in measured modulus in the flat clamping configuration was still over 29%. Manipulating a nanowire to

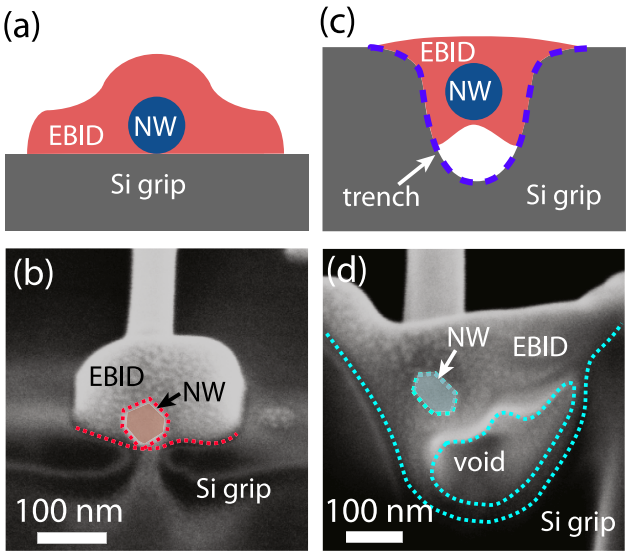

Figure 4. Schematics ((a), (c)) and SEM images ((b), (d)) of FIB-polished cross sections of Pd nanowires (NW) clamped to a flat surface ((a), (b)) and in a trench ((c), (d)). NWs in trenches do not often touch the bottom but rather make contact with side walls or remain suspended from nearby surfaces, whereas samples clamped to flat surfaces often make direct contact with the Si grips.

the trench geometry is generally more efficient and results in better alignment of the nanowires to the tensile axis, but only one of the trench-geometry tests shown here had error less than 10%.

This motivated several attempts to improve the stiffness of the trenched contacts. A common strategy within the electrical testing community is to improve contacts (i.e. increase electrical conductivity) by increasing their metal content. It has been shown that the resistivities of EBID deposits of a given material depend on electron accelerating voltage and beam current, which is ascribed to the primary influence of metal content [23, 31, 35]. Low electrical resistivity implies a percolating metal network, which would suggest an increase in contact stiffness since metals are stiffer than the surrounding amorphous carbonaceous matrix. For Pd F, Pt clamps were deposited at 2 kV and 420 pA, which has been reported to increase the metal content from approximately 5 at.% (10 or 20 kV and 40 pA) to 16 at.% [31], below the threshold of 30% by volume (approximately 17 at.%) for a percolating network [36] but sufficiently high to expect a lowering of electrical resistivity by as high as a factor of 4 [37]. Si E was clamped with W-containing EBID material, which is reported (albeit for much larger beam currents than employed in the current study) to have a metal content over 35 at.% [32], notably above the percolation threshold. Furthermore, bulk W has a Young's modulus more than double that of Pt. Further attempts included annealing a device with Si A (see table 1) attached in oxygen at 300 °C for 10 min to increase the metal concentration of the clamp following the methods of Botman *et al* [38], which has been shown to decrease the resistivity of the deposits by three orders of magnitude by removing the insulating carbon matrix from between the

Pt crystallites such that the metal content rises above the percolation threshold. Since the annealing step removed most of the contact material, additional material was then deposited on top, resulting in a contact with a significantly higher overall metal content. Taking these methods as a whole, no trend in contact stiffness with increased metal content was measured, implying that the percolation thresholds for electrical and stiff mechanical connectivity are indeed distinct. This suggests that the stiffness of these organometallic composite contacts is dominated by the organic matrix, consistent with the findings of Utke *et al* [39].

Since varying electron power density has been shown to affect deposition rate and metal content and furthermore shows a saturation in the metal content achievable in typical electron microscopes [31], the implication is that the elastic stiffness of the EBID material itself is inherently limited (unlike the contact strength as discussed earlier), and so the geometry of the deposit must be considered. Accordingly, the lengths of the contacts along the axes of the wires were varied for Si, but the contact stiffness showed no apparent relationship with contact length. Similarly, varying contact width from 470 nm for Pd C to 700 nm for Pd A resulted in nearly identical contact stiffnesses.

On the whole, these limitations on the maximum contact stiffness imply that accurate measurements of Young's modulus are favored on longer or thinner, and therefore more compliant, nanowires. The lowest measured contact stiffness was 0.57 kN m^{-1}; taking this as the minimum possible contact stiffness, the nanowire stiffness must be less than 0.03 kN m^{-1} to yield better than 90% accuracy in modulus measurement. For a nanowire with Young's modulus 100 GPa and diameter 100 nm, this implies a minimum gauge length of approximately 25 μm, longer than typical tensile testing specimens. This may explain the large scatter in the reported Young's moduli among distinct testing methods, as especially evident where tensile testing yields the lowest measured modulus [20] or is systematically lower than bulk values [10, 11]. Although usage of the apparent strain will only yield values of Young's modulus that are lower than the actual values, it is important to note that observation of nanowire moduli that are higher than bulk does not necessarily indicate that clamp effects are negligible. Indeed, in the case of Pd D, the apparent modulus was higher than bulk, whereas the actual modulus was higher still owing to size-dependent elasticity [14]. When a sufficiently compliant sample cannot be prepared, local strain measurements such as the method we have described here, selected area diffraction [9], or Raman spectroscopy [40–43], should be used. Other methods of attaching nanowires to tensile testing setups should also be considered, e.g. deposition of pure metal or semiconductor contact materials by evaporation through a shadow mask, co-fabrication of specimens directly onto testing apparatuses [44], or nanoscale spot welding [45–47].

4. Conclusion

In summary, we have shown that the EBID clamps commonly used for nanoscale tensile testing have stiffnesses that are approximately on the order of the stiffness of inorganic nanowire specimens commonly tested. As a consequence, inconsistent and significant errors—as high as 39% and as low as 1%—are introduced in measurements of displacement and hence strain and Young's modulus, with a strong dependence on the stiffness of the sample and the geometry of the clamp. Furthermore, permanent clamp deformation resulted in nominal stress–strain curves that incorrectly indicated plastic deformation in the nanowires. We have demonstrated that a local measurement of strain is a necessity for mechanical testing when EBID clamps are used. Our work may explain anomalous behaviors and discrepancies between nanowire moduli measured using grip displacement and provides guidelines for the nanowire and clamp stiffnesses needed to achieve acceptable errors in measurements of strain.

Acknowledgments

This research was supported by the US Department of Energy, Office of Basic Energy Sciences, Division of Materials Science and Engineering under Award No. DE-SC0008135 (semiconductor nanowires) and the National Science Foundation through a CAREER Award No. DMR-1056293 (metallic nanowires). We acknowledge additional support through start-up funding from the University of Pennsylvania. We thank J P Sullivan for providing the MEMS testing devices and for technical support, G Richter for providing Pd nanowhiskers, and R Agarwal for providing $Ge_2Sb_2Te_5$ nanowires. The authors also thank the support of the staff and facilities at the Penn Regional Nanotechnology Facility at the University of Pennsylvania. This work was performed, in part, at the Center for Integrated Nanotechnologies, a US Department of Energy, Office of Basic Energy Sciences user facility. Sandia National Laboratories is a multi-program laboratory managed and operated by Sandia Corporation, a wholly owned subsidiary of Lockheed Martin Corporation, for the US Department of Energy's National Nuclear Security Administration under contract DE-AC04-94AL85000.

References

[1] Peng K, Jie J, Zhang W and Lee S-T 2008 Silicon nanowires for rechargeable lithium-ion battery anodes *Appl. Phys. Lett.* **93** 033105

[2] Liu X H *et al* 2011 Anisotropic swelling and fracture of silicon nanowires during lithiation *Nano Lett.* **11** 3312–8

[3] Boles S T, Sedlmayr A, Kraft O and Mönig R 2012 *In situ* cycling and mechanical testing of silicon nanowire anodes for lithium-ion battery applications *Appl. Phys. Lett.* **100** 243901

[4] Cheung C L, Hafner J H and Lieber C M 2000 Carbon nanotube atomic force microscopy tips: direct growth by chemical vapor deposition and application to high-resolution imaging *Proc. Natl Acad. Sci.* **97** 3809–13

[5] Nagy G, Levy M, Scarmozzino R, Osgood R M Jr, Dai H, Smalley R E, Michaels C A, Flynn G W and McLane G F 1998 Carbon nanotube tipped atomic force microscopy for measurement of <100 nm etch morphology on semiconductors *Appl. Phys. Lett.* **73** 529

[6] Brodard P, Bechelany M, Philippe L and Michler J 2012 Synthesis and attachment of silver nanowires on atomic force microscopy cantilevers for tip-enhanced Raman spectroscopy *J. Raman Spectrosc.* **43** 745–9

[7] Zhu Y and Espinosa H D 2005 An electromechanical material testing system for *in situ* electron microscopy and applications *Proc. Natl Acad. Sci.* **102** 14503–8

[8] Lu S, Guo Z, Ding W, Dikin D A, Lee J and Ruoff R S 2006 *In situ* mechanical testing of templated carbon nanotubes *Rev. Sci. Instrum.* **77** 125101

[9] Agrawal R, Peng B, Gdoutos E E and Espinosa H D 2008 Elasticity size effects in ZnO nanowires—a combined experimental-computational approach *Nano Lett.* **8** 3668–74

[10] Zhang D, Breguet J-M, Clavel R, Sivakov V, Christiansen S and Michler J 2010 *In situ* electron microscopy mechanical testing of silicon nanowires using electrostatically actuated tensile stages *J. Microelectromech. Syst.* **19** 663–74

[11] Zhang Y L Y, Liu X, Ru C, Zhang Y L, Dong L and Sun Y 2011 Piezoresistivity characterization of synthetic silicon nanowires using a MEMS device *J. Microelectromech. Syst.* **20** 959–67

[12] Pant B, Allen B L, Zhu T, Gall K and Pierron O N 2011 A versatile microelectromechanical system for nanomechanical testing *Appl. Phys. Lett.* **98** 053506

[13] Gianola D S, Sedlmayr A, Mönig R, Volkert C A, Major R C, Cyrankowski E, Asif S a S, Warren O L and Kraft O 2011 *In situ* nanomechanical testing in focused ion beam and scanning electron microscopes *Rev. Sci. Instrum.* **82** 063901

[14] Chen L, Richter G, Sullivan J and Gianola D 2012 Lattice anharmonicity in defect-free Pd nanowhiskers *Phys. Rev. Lett.* **109** 125503

[15] Lu Y, Ganesan Y and Lou J 2010 A multi-step method for *in situ* mechanical characterization of 1-D nanostructures using a novel micromechanical device *Exp. Mech.* **50** 47–54

[16] Guo H, Chen K, Oh Y, Wang K, Dejoie C, Syed Asif S A, Warren O L, Shan Z W, Wu J and Minor A M 2011 Mechanics and dynamics of the strain-induced M1–M2 structural phase transition in individual VO_2 nanowires *Nano Lett.* **11** 3207–13

[17] Chisholm C, Bei H, Lowry M B, Oh J, Syed Asif S A, Warren O L, Shan Z W, George E P and Minor A M 2012 Dislocation starvation and exhaustion hardening in Mo alloy nanofibers *Acta Mater.* **60** 2258–64

[18] Zhu Y, Xu F, Qin Q, Fung W Y and Lu W 2009 Mechanical properties of vapor–liquid–solid synthesized silicon nanowires *Nano Lett.* **9** 3934–9

[19] Richter G, Hillerich K, Gianola D S, Mönig R, Kraft O and Volkert C A 2009 Ultrahigh strength single crystalline nanowhiskers grown by physical vapor deposition *Nano Lett.* **9** 3048–52

[20] Xu F, Qin Q, Mishra A, Gu Y and Zhu Y 2010 Mechanical properties of ZnO nanowires under different loading modes *Nano Res.* **3** 271–80

[21] Zhu Y, Qin Q, Xu F, Fan F, Ding Y, Zhang T, Wiley B J and Wang Z L 2012 Size effects on elasticity, yielding, and fracture of silver nanowires: *in situ* experiments *Phys. Rev.* B **85** 045443

[22] Yu M-F, Lourie O, Dyer M J, Moloni K, Kelly T F and Ruoff R S 2000 Strength and breaking mechanism of multiwalled carbon nanotubes under tensile load *Science* **287** 637–40

[23] Van Dorp W F and Hagen C W 2008 A critical literature review of focused electron beam induced deposition *J. Appl. Phys.* **104** 081301

[24] Ding W, Dikin D A, Chen X, Piner R D, Ruoff R S, Zussman E, Wang X and Li X 2005 Mechanics of hydrogenated amorphous carbon deposits from electron-beam-induced deposition of a paraffin precursor *J. Appl. Phys.* **98** 014905

[25] Friedli V, Utke I, Mølhave K and Michler J 2009 Dose and energy dependence of mechanical properties of focused electron-beam-induced pillar deposits from $Cu(C_5HF_6O_2)_2$ *Nanotechnology* **20** 385304

[26] Qin Q, Xu F, Cao Y, Ro P I and Zhu Y 2012 Measuring true Young's modulus of a cantilevered nanowire: effect of clamping on resonance frequency *Small* **8** 2571–6

[27] Choi W K, Liew T H, Dawood M K, Smith H I, Thompson C V and Hong M H 2008 Synthesis of silicon nanowires and nanofin arrays using interference lithography and catalytic etching *Nano Lett.* **8** 3799–802

[28] Lee D H, Kim Y, Doerk G S, Laboriante I and Maboudian R 2011 Strategies for controlling Si nanowire formation during Au-assisted electroless etching *J. Mater. Chem.* **21** 10359

[29] Jung Y, Lee S-H, Ko D-K and Agarwal R 2006 Synthesis and characterization of $Ge_2Sb_2Te_5$ nanowires with memory switching effect *J. Am. Chem. Soc.* **128** 14026–7

[30] Lee S-H, Jung Y and Agarwal R 2007 Highly scalable non-volatile and ultra-low-power phase-change nanowire memory *Nat. Nanotechnol.* **2** 626–30

[31] Botman A, Hesselberth M and Mulders J J L 2008 Improving the conductivity of platinum-containing nano-structures created by electron-beam-induced deposition *Microelectron. Eng.* **85** 1139–42

[32] Mulders J J L, Belova L M and Riazanova A 2011 Electron beam induced deposition at elevated temperatures: compositional changes and purity *Nanotechnology* **22** 055302

[33] Guo Q, Li M, Li Y, Shi L, Chong T C, Kalb J A and Thompson C V 2008 Crystallization-induced stress in thin phase change films of different thicknesses *Appl. Phys. Lett.* **93** 221907

[34] Park I-M, Jung J-K, Ryu S-O, Choi K-J, Yu B-G, Park Y-B, Han S M and Joo Y-C 2008 Thermomechanical properties and mechanical stresses of $Ge_2Sb_2Te_5$films in phase-change random access memory *Thin Solid Films* **517** 848–52

[35] Koops H W P, Kaya A and Weber M 1995 Fabrication and characterization of platinum nanocrystalline material grown by electronbeam induced deposition *J. Vac. Sci. Technol.* B **13** 2400–3

[36] Pike G E and Seager C H 1974 Percolation and conductivity: a computer study. I *Phys. Rev.* B **10** 1421–34

[37] Schossler C, Kaya A, Kretz J, Weber M and Koops H W P 1996 Electrical and field emission properties of nanocrystalline materials fabricated by electron-beam induced deposition *Microelectron. Eng.* **30** 471–4

[38] Botman A, Mulders J J L, Weemaes R and Mentink S 2006 Purification of platinum and gold structures after electron-beam-induced deposition *Nanotechnology* **17** 3779–85

[39] Utke I, Friedli V, Fahlbusch S, Hoffmann S, Hoffmann P and Michler J 2006 Tensile strengths of metal-containing joints fabricated by focused electron beam induced deposition *Adv. Eng. Mater.* **8** 155–7

[40] De Wolf I 1996 Micro-Raman spectroscopy to study local mechanical stress in silicon integrated circuits *Semicond. Sci. Technol.* **11** 139–54

[41] Wermelinger T, Charpentier C, Yuksek M D and Spolenak R 2009 Measuring stresses in thin metal films by means of Raman microscopy using silicon as a strain gage material *J. Raman Spectrosc.* **40** 1849–57

[42] Wasmer K, Wermelinger T, Bidiville A, Spolenak R and Michler J 2011 *In situ* compression tests on micron-sized silicon pillars by Raman microscopy—stress measurements and deformation analysis *J. Mater. Res.* **23** 3040–7

[43] Greil J, Lugstein A, Zeiner C, Strasser G and Bertagnolli E 2012 Tuning the electro-optical properties of germanium nanowires by tensile strain *Nano Lett.* **12** 6230–4

[44] He R and Yang P 2006 Giant piezoresistance effect in silicon nanowires *Nature Nanotechnol.* **1** 42–6

[45] Tohmyoh H, Imaizumi T, Hayashi H and Saka M 2007 Welding of Pt nanowires by Joule heating *Scr. Mater.* **57** 953–6

[46] Lu Y, Huang J Y, Wang C, Sun S and Lou J 2010 Cold welding of ultrathin gold nanowires *Nature Nanotechnol.* **5** 218–24

[47] Martinez J A, Provencio P P, Picraux S T, Sullivan J P and Swartzentruber B S 2011 Enhanced thermoelectric figure of merit in SiGe alloy nanowires by boundary and hole-phonon scattering *J. Appl. Phys.* **110** 074317